ChemComm

RSC Publishing

COMMUNICATION

View Article Online
View Journal | View Issue

Hierarchical $NiCo_2O_4$@MnO_2 core–shell heterostructured nanowire arrays on Ni foam as high-performance supercapacitor electrodes†

Cite this: *Chem. Commun.*, 2013, **49**, 137

Received 30th September 2012, Accepted 6th November 2012

DOI: 10.1039/c2cc37117k

www.rsc.org/chemcomm

Le Yu,‡ Genqiang Zhang,‡ Changzhou Yuan* and Xiong Wen (David) Lou*

Published on 06 novembre 2012. Downloaded on 17/11/2025 23:47:56.

An advanced integrated electrode for high-performance supercapacitors has been designed by growing hierarchical $NiCo_2O_4$@MnO_2 core–shell heterostructured nanowire arrays on nickel foam. Such unique array nanoarchitectures exhibit remarkable electrochemical performance with high capacitance and desirable cycle life at high rates.

With increasing demand in electric energy storage for electric vehicles and mobile electronics, supercapacitors have attracted extensive research interest because of their high power density, fast recharge capability and long cycle life.[1] When reversible Faradaic redox reactions are introduced at the electrode/electrolyte interfaces, a pseudocapacitor electrode is formed, which has area specific capacitance (ASC) considerably exceeding that of carbon-based supercapacitors (low ASC of 10–40 μF cm^{-2})[2] based on electrical double-layer charge storage. Thus, transition metal oxides with variable valence have been widely investigated as candidates for use in supercapacitors in view of their multiple oxidation states for pseudocapacitance generation. However, due to the intrinsic poor electrical conductivity of metal oxides and the short diffusion distance (~20 nm) of electrolytes into pseudocapacitor electrodes,[3] only the surface part of electroactive materials can effectively contribute to the total capacitance and the underneath parts could hardly participate in the electrochemical charge storage process, leading to a less satisfactory ASC. Therefore, it is still a great challenge to boost the electrochemical utilization and ASC of pseudocapacitive materials by rationally designing electrodes with novel microstructures. An emerging attractive concept is to directly grow smart integrated array architectures with the combination of two types of materials and/or nanostructures on conducting substrates as binder-free electrodes for supercapacitors.[4–14] In this way, many competitive advantages such as rich accessible electroactive sites, short ion transport pathways, superior electron collection efficiency, and even fascinating synergetic properties or multifunctionalities of components are simultaneously achieved to deliver high ASC, desirable cycle life and rate performance.

Recently, ternary $NiCo_2O_4$[15–20] and MnO_2[21–24] have been the two most widely investigated pseudocapacitive materials due to their low cost, environmentally benign nature, natural abundance and high theoretical capacitance. Particularly, $NiCo_2O_4$ possesses much better electrical conductivity and higher redox activity compared to nickel oxides and cobalt oxides.[15–20] But till now, there is no study on electrochemical capacitance of their integrated electrodes with the aim to boost ASC by rationally combining merits of $NiCo_2O_4$ and MnO_2, although the individual capacitive property of both has been extensively investigated.

In this communication, we develop a cost-effective and simple strategy to design and fabricate novel hierarchical $NiCo_2O_4$@MnO_2 core–shell heterostructured nanowire (NW) arrays on Ni foam as a binder-free electrode for high-performance supercapacitors, where the slim mesoporous $NiCo_2O_4$ NWs are the "core" and ultrathin MnO_2 nanoflakes the "shell" layer. The smartly designed core–shell heterostructured NW arrays on Ni foam, when applied as an electrode, own multiple apparent advantages as follows: (I) ultrathin MnO_2 nanoflakes are well wrapped on $NiCo_2O_4$ NW surfaces, which would enable a fast, reversible Faradaic reaction, and provide a short ion diffusion path and maintain the structural integrity of the core during charge–discharge process; (II) slim and mesoporous $NiCo_2O_4$ NWs with good electrical conductivity directly grown on conductive Ni foam serve both as the backbone and electron "superhighway" for charge storage and delivery, overcoming the limited electrical conductivity of MnO_2 itself, and the mesoporous feature leads to a large electrode/electrolyte contact interface; (III) both the core and shell materials are good pseudocapacitive materials, which undergo redox reactions with anions and cations in the electrolyte, hence contributing to the electrochemical energy storage; (IV) the core–shell heterostructured NWs are well separated and strongly supported on Ni foam, avoiding the use of polymer binder/conductive additives and ensuring a sufficiently porous structure, and consequently the "inactive" surface is significantly reduced. Thus, all the desired functions

School of Chemical and Biomedical Engineering, Nanyang Technological University, 62 Nanyang Drive, Singapore 637459. E-mail: czyuan@ntu.edu.sg, xwlou@ntu.edu.sg; Web: http://www.ntu.edu.sg/home/xwlou/

† Electronic supplementary information (ESI) available: The detailed synthesis conditions, EDX and impedance spectra and other SEM/TEM images. See DOI: 10.1039/c2cc37117k

‡ These authors contributed equally to this work.

Published on 06 novembre 2012. Downloaded on 17/11/2025 23:47:56.

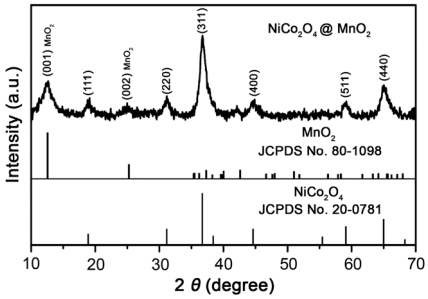

Fig. 1 XRD pattern of hierarchical $NiCo_2O_4$@MnO_2 core–shell heterostructured NW arrays scratched from Ni foam.

of each constituent are efficiently utilized to realize a strong synergistic effect. Impressively, the optimal $NiCo_2O_4$@MnO_2 core–shell heterostructured NW arrays exhibit large ASC of 3.31 F cm^{-2}, desirable rate performance and cycling stability in a 1 M LiOH solution.

Hierarchical $NiCo_2O_4$@MnO_2 core–shell heterostructured NW arrays are synthesized *via* a two-step solution route coupled with a post calcination treatment. The detailed preparation procedure can be found in the ESI.† In order to reduce the strong impact of the Ni foam substrate on the XRD peak signals (ESI,† Fig. S1), the $NiCo_2O_4$@MnO_2 core–shell heterostructured NW powder is scratched from Ni foam for XRD analysis. As shown in Fig. 1, the XRD pattern confirms the existence of the spinel $NiCo_2O_4$ phase (JCPDF card no. 20-0781) and crystalline birnessite-type MnO_2 (JCPDF card no. 80-1098). The energy dispersive X-ray spectroscopy (EDX) data (ESI,† Fig. S2) further verify the Mn species present in the core–shell arrays.

Fig. 2a and b demonstrate the top-view field-emission scanning electron microscopy (FESEM) images of the $NiCo_2O_4$ NW arrays grown on Ni foam. Obviously, the slim $NiCo_2O_4$ NWs with sharp tips are homogeneously aligned and separated apart adequately, forming a unique nanoarray with a highly open and porous structure on a large scale (ESI,† Fig. S3a). Fig. 2c and d show the typical FESEM images of final $NiCo_2O_4$@MnO_2 core–shell NW arrays grown on Ni foam. Clearly, no MnO_2 is packed in the interspace of the NWs, suggesting that MnO_2 nanoflakes are preferentially deposited on the

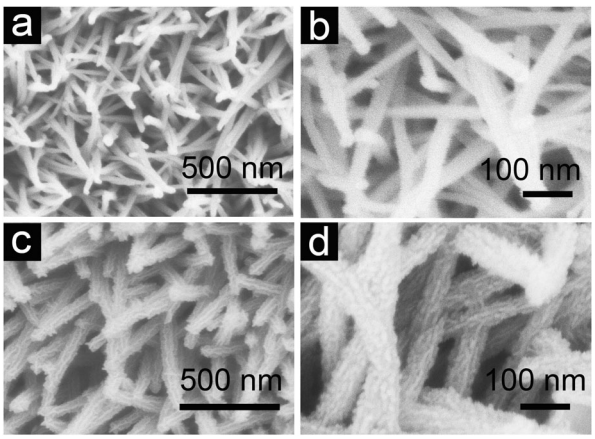

Fig. 2 FESEM images of (a, b) $NiCo_2O_4$ NW arrays and (c, d) hierarchical $NiCo_2O_4$@MnO_2 core–shell heterostructured NW arrays grown on Ni foam.

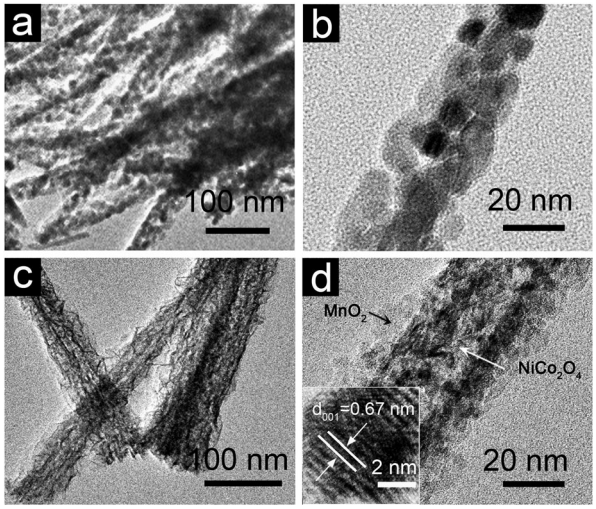

Fig. 3 TEM images of (a, b) $NiCo_2O_4$ NWs and (c, d) $NiCo_2O_4$@MnO_2 core–shell heterostructured NWs scratched from Ni foam. The inset of (d) shows a HRTEM image of MnO_2 nanoflakes.

$NiCo_2O_4$ NW surface. Thus, the uniform coverage of MnO_2 nanoflakes on each $NiCo_2O_4$ NW surface can be seen. Of importance, even with two components integrated, the uniform array structure is still well retained (ESI,† Fig. S3b). Thus, nearly all the core–shell NWs are highly accessible to electrolytes for energy storage due to the presence of convenient diffusion channels.

As can be seen in the TEM images of the $NiCo_2O_4$ NWs (Fig. 3a and b), these needle-like NWs are highly porous, composed of nanocrystallites of 7–10 nm in size and mesopores of 3–5 nm. From Fig. 3c and d, it is evidently observed that the mesoporous $NiCo_2O_4$ "nanocore" is tightly bonded and totally covered with leaf-like ultrathin MnO_2 nanoflakes, forming a typical core–shell heterostructured architecture. A close examination of the exposed profile reveals that the thickness of the outer symmetric MnO_2 shell layer is about 10 nm. Moreover, the thickness of the MnO_2 shell can be easily varied by controlling the concentration of $KMnO_4$ solution (ESI,† Fig. S4). The high resolution TEM (HRTEM) examination shown in Fig. 3d reveals a distinct set of visible lattice fringes with an inter-planar spacing of 0.67 nm, corresponding to the (001) plane of birnessite-type MnO_2.

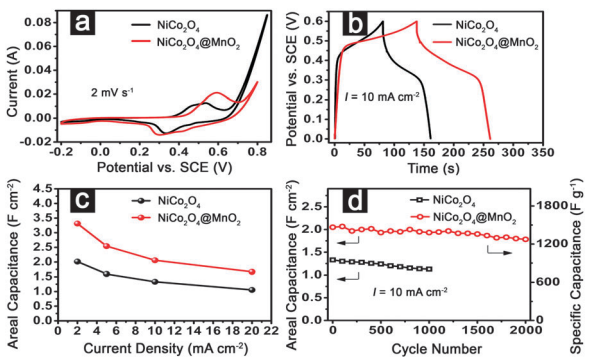

Fig. 4 (a) CV curves, (b) CP plots, (c) areal capacitances and (d) capacitance as a function of cycle number for $NiCo_2O_4$ NW arrays and hierarchical $NiCo_2O_4$@MnO_2 core–shell NW arrays on Ni foam.

 This journal is © The Royal Society of Chemistry 2013

Published on 06 novembre 2012. Downloaded on 17/11/2025 23:47:56.

Next, we directly applied the hierarchical $NiCo_2O_4$@MnO_2 core–shell heterostructured NW arrays on Ni foam as an integrated electrode to highlight the merits of the unique architecture in a three-electrode configuration with 1 M LiOH as the electrolyte. Fig. 4a shows the cyclic voltammograms (CVs) of the $NiCo_2O_4$, and $NiCo_2O_4$@MnO_2 core–shell NW arrays supported on Ni foam at a scan rate of 2 mV s^{-1}. Apparently, a pair of redox peaks is observed for the $NiCo_2O_4$ NW array electrode, which originates from Faradaic reactions related to M–O/M–O–OH (M represents Ni and Co ions) associated with anions OH^-.[15,16,20] Remarkably, a similar CV shape is still found for the core–shell NW arrays, indicating the efficient utilization of the underlying $NiCo_2O_4$ nanorods despite covered by the MnO_2 nanoflakes, while the area integrated within the current–potential curves greatly increases for the core–shell NW arrays, leading to a much larger pseudocapacitance. It should be attributed to the additional pseudocapacitance contributed by the MnO_2 shell, which can adsorb Li^+ cations on the electrode surface and/or possibly intercalate and deintercalate Li^+ ions.[6,25] Also, upon increasing the scan rates up to 50 mV s^{-1}, the CV curves vary little (ESI,† Fig. S5a), revealing the excellent high-rate performance of the unique core–shell NW arrays. Furthermore, the coating of MnO_2 nanoflakes leads to reduced charge transfer resistance of the hybrid arrays (ESI,† Fig. S6), which may further enhance the electrochemical performance.

Galvanostatic charge–discharge measurements are further performed in the voltage range between 0 and 0.6 V (*vs.* SCE) to estimate the ASC of electrode materials. As shown in Fig. 4b, evidently, the $NiCo_2O_4$@MnO_2 core–shell NW arrays deliver higher ASC than $NiCo_2O_4$ NW arrays. Also, the ASC of the core–shell heterostructured NW arrays can be calculated based on the chronopotentiometry (CP) curves (ESI,† Fig. S5b) and typical data are presented in Fig. 4c. Impressively, the Ni foam-supported core–shell heterostructured NW array electrode delivers higher ASC of 3.31, 2.54, 2.06 and 1.66 F cm^{-2} at current densities of 2, 5, 10 and 20 mA cm^{-2}, respectively, compared to only 2.01 and 1.05 F cm^{-2} at 2 and 20 mA cm^{-2}, respectively, for the $NiCo_2O_4$ NW arrays. Furthermore, the ASC reported here is much higher than those of conventional carbonaceous materials,[2,3] and even higher than those of previously reported directly-grown pseudocapacitive array nanoarchitectures, such as NiO–TiO_2 nanotube arrays (3 F cm^{-2} at 0.4 mA cm^{-2}),[10] Co_3O_4–MnO_2 NW/nanosheet core–shell arrays (0.56 F cm^{-2} at 11.25 mA cm^{-2}),[6] Co_3O_4–NiO core–shell NW arrays (1.35 F cm^{-2} at 6 mA cm^{-2}),[5] MnO_2–NiO core–shell NW arrays (0.35 F cm^{-2} at 9.5 mA cm^{-2}),[7] *etc.* Such high ASC at large current densities further proves the great advantages of the present core–shell heterostructured NW arrays.

The electrochemical stability of $NiCo_2O_4$@MnO_2 core–shell NW arrays is examined by repeated charging–discharging processes. As shown in Fig. 4d, it is clear that both the ASC and cycling stability are largely enhanced in the core–shell NW array electrode. The ASC increases from 1.33 F cm^{-2} for the bare $NiCo_2O_4$ NW arrays to 2.05 F cm^{-2} for the core–shell NW arrays. The overall capacitance loss for $NiCo_2O_4$ NW arrays is about 15% after 1000 cycles, while it is only 12% even after 2000 cycles for the core–shell NW arrays. The specific capacitance degradation of the core–shell NW arrays is estimated to be from 1471.4 to 1273.8 F g^{-1} (right vertical axis, Fig. 4d). Thus, the unique array electrode shows high electrochemical stability for long cycle life applications at high current densities.

In conclusion, a facile and scalable strategy has been developed to construct hierarchical $NiCo_2O_4$@MnO_2 core–shell heterostructured NW array nanoarchitectures with high electrochemical performance for supercapacitors. The as-fabricated core–shell heterostructured NW array electrode delivers high capacitance of 1.66 F cm^{-2} even at 20 mA cm^{-2} and desirable rate performance and electrochemical stability. Such intriguing capacitive behavior is attributed to the unique hierarchical core–shell heterostructured NW array configuration and the synergistic effects of the combined pseudocapacitive contributions from the mesoporous $NiCo_2O_4$ NW core and the ultrathin MnO_2 shell layer. This work again confirms the feasibility of rational design of advanced integrated array electrode materials for high-performance supercapacitors.

Notes and references

1 P. Simon and Y. Gogotsi, *Nat. Mater.*, 2008, **7**, 845; J. R. Miller and P. Simon, *Science*, 2008, **321**, 651.
2 M. Salari, S. H. Aboutalebi, K. Konstantinov and H. K. Liu, *Phys. Chem. Chem. Phys.*, 2011, **13**, 5038; C. Guan, X. L. Li, Z. L. Wang, X. H. Cao, C. Soci, H. Zhang and H. J. Fan, *Adv. Mater.*, 2012, **24**, 4186.
3 C. C. Hu, K. H. Chang, M. C. Lin and Y. T. Wu, *Nano Lett.*, 2006, **6**, 2690; Z. Y. Lu, Q. Yang, W. Zhu, Z. Chang, J. F. Liu, X. M. Sun, D. G. Evans and X. Duan, *Nano Res.*, 2012, **5**, 369.
4 X. H. Lu, T. Zhai, X. H. Zhang, Y. Q. Shen, L. Y. Yuan, B. Hu, L. Gong, J. Chen, Y. H. Gao, J. Zhou, Y. X. Tong and Z. L. Wang, *Adv. Mater.*, 2012, **24**, 938.
5 X. H. Xia, J. P. Tu, Y. Q. Zhang, X. L. Wang, C. D. Gu, X. B. Zhao and H. J. Fan, *ACS Nano*, 2012, **6**, 5531.
6 J. P. Liu, J. Jiang, C. W. Cheng, H. X. Li, J. X. Zhang, H. Gong and H. J. Fan, *Adv. Mater.*, 2011, **23**, 2076.
7 J. P. Liu, J. Jiang, M. Bosman and H. J. Fan, *J. Mater. Chem.*, 2012, **22**, 2419.
8 H. Jiang, C. Z. Li, T. Sun and J. Ma, *Chem. Commun.*, 2012, **48**, 2606.
9 G. R. Li, Z. L. Wang, F. L. Zheng, Y. N. Ou and Y. X. Tong, *J. Mater. Chem.*, 2011, **21**, 4217.
10 J. H. Kim, K. Zhu, Y. F. Yan, C. L. Perkins and A. J. Frank, *Nano Lett.*, 2010, **10**, 4099.
11 J. Jiang, Y. Y. Li, J. P. Liu, X. T. Huang, C. Z. Yuan and X. W. Lou, *Adv. Mater.*, 2012, **24**, 5166.
12 L. Q. Mai, F. Yang, Y. L. Zhao, X. Xu, L. Xu and Y. Z. Luo, *Nat. Commun.*, 2011, **2**, 2041.
13 J. A. Yan, E. Khoo, A. Sumboja and P. S. Lee, *ACS Nano*, 2010, **4**, 4247.
14 L. H. Bao, J. F. Zang and X. D. Li, *Nano Lett.*, 2011, **11**, 1215.
15 T. Y. Wei, C. H. Chen, H. C. Chien, S. Y. Lu and C. C. Hu, *Adv. Mater.*, 2010, **22**, 347.
16 H. L. Wang, Q. M. Gao and L. Jiang, *Small*, 2011, **7**, 2454.
17 H. Jiang, J. Ma and C. Z. Li, *Chem. Commun.*, 2012, **48**, 4465.
18 H. W. Wang, Z. A. Hu, Y. Q. Chang, Y. L. Chen, H. Y. Wu, Z. Y. Zhang and Y. Y. Yang, *J. Mater. Chem.*, 2011, **21**, 10504.
19 G. Q. Zhang, H. B. Wu, H. E. Hoster, M. B. Chan-park and X. W. Lou, *Energy Environ. Sci.*, 2012, **5**, 9453.
20 C. Z. Yuan, J. Y. Li, L. R. Hou, X. G. Zhang, L. F. Shen and X. W. Lou, *Adv. Funct. Mater.*, 2012, **22**, 4592.
21 Y. K. Hsu, Y. C. Chen, Y. G. Lin, L. C. Chen and K. H. Chen, *Chem. Commun.*, 2011, **47**, 1252.
22 W. Lee, J. Kim, S. Chen, P. T. Hammond and Y. Shao-Horn, *ACS Nano*, 2010, **4**, 3889.
23 Q. Li, Z. L. Wang, G. R. Li, R. Guo, L. X. Ding and Y. X. Tong, *Nano Lett.*, 2012, **12**, 3803.
24 X. H. Tang, H. J. Li, Z. H. Liu, Z. P. Yang and Z. L. Wang, *J. Power Sources*, 2011, **196**, 855.
25 D. Blanger, T. Brousse and J. W. Long, *Electrochem. Soc. Interface*, 2008, **17**, 49.